Search for the Higgs boson in the all-hadronic final state using the CDF II detector

T. Aaltonen,[21] B. Álvarez González[v],[9] S. Amerio,[41] D. Amidei,[32] A. Anastassov,[36] A. Annovi,[17] J. Antos,[12] G. Apollinari,[15] J.A. Appel,[15] A. Apresyan,[46] T. Arisawa,[56] A. Artikov,[13] J. Asaadi,[51] W. Ashmanskas,[15] B. Auerbach,[59] A. Aurisano,[51] F. Azfar,[40] W. Badgett,[15] A. Barbaro-Galtieri,[26] V.E. Barnes,[46] B.A. Barnett,[23] P. Barria[cc],[44] P. Bartos,[12] M. Bauce[aa],[41] G. Bauer,[30] F. Bedeschi,[44] D. Beecher,[28] S. Behari,[23] G. Bellettini[bb],[44] J. Bellinger,[58] D. Benjamin,[14] A. Beretvas,[15] A. Bhatti,[48] M. Binkley,[15] D. Bisello[aa],[41] I. Bizjak[gg],[28] K.R. Bland,[5] B. Blumenfeld,[23] A. Bocci,[14] A. Bodek,[47] D. Bortoletto,[46] J. Boudreau,[45] A. Boveia,[11] B. Brau[a],[15] L. Brigliadori[z],[6] A. Brisuda,[12] C. Bromberg,[33] E. Brucken,[21] M. Bucciantonio[bb],[44] J. Budagov,[13] H.S. Budd,[47] S. Budd,[22] K. Burkett,[15] G. Busetto[aa],[41] P. Bussey,[19] A. Buzatu,[31] C. Calancha,[29] S. Camarda,[4] M. Campanelli,[33] M. Campbell,[32] F. Canelli[12],[15] A. Canepa,[43] B. Carls,[22] D. Carlsmith,[58] R. Carosi,[44] S. Carrillo[k],[16] S. Carron,[15] B. Casal,[9] M. Casarsa,[15] A. Castro[z],[6] P. Catastini,[15] D. Cauz,[52] V. Cavaliere[cc],[44] M. Cavalli-Sforza,[4] A. Cerri[f],[26] L. Cerrito[q],[28] Y.C. Chen,[1] M. Chertok,[7] G. Chiarelli,[44] G. Chlachidze,[15] F. Chlebana,[15] K. Cho,[25] D. Chokheli,[13] J.P. Chou,[20] W.H. Chung,[58] Y.S. Chung,[47] C.I. Ciobanu,[42] M.A. Ciocci[cc],[44] A. Clark,[18] G. Compostella[aa],[41] M.E. Convery,[15] J. Conway,[7] M.Corbo,[42] M. Cordelli,[17] C.A. Cox,[7] D.J. Cox,[7] F. Crescioli[bb],[44] C. Cuenca Almenar,[59] J. Cuevas[v],[9] R. Culbertson,[15] D. Dagenhart,[15] N. d'Ascenzo[t],[42] M. Datta,[15] P. de Barbaro,[47] S. De Cecco,[49] G. De Lorenzo,[4] M. Dell'Orso[bb],[44] C. Deluca,[4] L. Demortier,[48] J. Deng[c],[14] M. Deninno,[6] F. Devoto,[21] M. d'Errico[aa],[41] A. Di Canto[bb],[44] B. Di Ruzza,[44] J.R. Dittmann,[5] M. D'Onofrio,[27] S. Donati[bb],[44] P. Dong,[15] M. Dorigo,[52] T. Dorigo,[41] K. Ebina,[56] A. Elagin,[51] A. Eppig,[32] R. Erbacher,[7] D. Errede,[22] S. Errede,[22] N. Ershaidat[y],[42] R. Eusebi,[51] H.C. Fang,[26] S. Farrington,[40] M. Feindt,[24] J.P. Fernandez,[29] C. Ferrazza[dd],[44] R. Field,[16] G. Flanagan[r],[46] R. Forrest,[7] M.J. Frank,[5] M. Franklin,[20] J.C. Freeman,[15] Y. Funakoshi,[56] I. Furic,[16] M. Gallinaro,[48] J. Galyardt,[10] J.E. Garcia,[18] A.F. Garfinkel,[46] P. Garosi[cc],[44] H. Gerberich,[22] E. Gerchtein,[15] S. Giagu[ee],[49] V. Giakoumopoulou,[3] P. Giannetti,[44] K. Gibson,[45] C.M. Ginsburg,[15] N. Giokaris,[3] P. Giromini,[17] M. Giunta,[44] G. Giurgiu,[23] V. Glagolev,[13] D. Glenzinski,[15] M. Gold,[35] D. Goldin,[51] N. Goldschmidt,[16] A. Golossanov,[15] G. Gomez,[9] G. Gomez-Ceballos,[30] M. Goncharov,[30] O. González,[29] I. Gorelov,[35] A.T. Goshaw,[14] K. Goulianos,[48] A. Gresele,[41] S. Grinstein,[4] C. Grosso-Pilcher,[11] R.C. Group,[55] J. Guimaraes da Costa,[20] Z. Gunay-Unalan,[33] C. Haber,[26] S.R. Hahn,[15] E. Halkiadakis,[50] A. Hamaguchi,[39] J.Y. Han,[47] F. Happacher,[17] K. Hara,[53] D. Hare,[50] M. Hare,[54] R.F. Harr,[57] K. Hatakeyama,[5] C. Hays,[40] M. Heck,[24] J. Heinrich,[43] M. Herndon,[58] S. Hewamanage,[5] D. Hidas,[50] A. Hocker,[15] W. Hopkins[g],[15] D. Horn,[24] S. Hou,[1] R.E. Hughes,[37] M. Hurwitz,[11] U. Husemann,[59] N. Hussain,[31] M. Hussein,[33] J. Huston,[33] G. Introzzi,[44] M. Iori[ee],[49] A. Ivanov[o],[7] E. James,[15] D. Jang,[10] B. Jayatilaka,[14] E.J. Jeon,[25] M.K. Jha,[6] S. Jindariani,[15] W. Johnson,[7] M. Jones,[46] K.K. Joo,[25] S.Y. Jun,[10] T.R. Junk,[15] T. Kamon,[51] P.E. Karchin,[57] Y. Kato[n],[39] W. Ketchum,[11] J. Keung,[43] V. Khotilovich,[51] B. Kilminster,[15] D.H. Kim,[25] H.S. Kim,[25] H.W. Kim,[25] J.E. Kim,[25] M.J. Kim,[17] S.B. Kim,[25] S.H. Kim,[53] Y.K. Kim,[11] N. Kimura,[56] M. Kirby,[15] S. Klimenko,[16] K. Kondo,[56] D.J. Kong,[25] J. Konigsberg,[16] A.V. Kotwal,[14] M. Kreps,[24] J. Kroll,[43] D. Krop,[11] N. Krumnack[l],[5] M. Kruse,[14] V. Krutelyov[d],[51] T. Kuhr,[24] M. Kurata,[53] S. Kwang,[11] A.T. Laasanen,[46] S. Lami,[44] S. Lammel,[15] M. Lancaster,[28] R.L. Lander,[7] K. Lannon[u],[37] A. Lath,[50] G. Latino[cc],[44] I. Lazzizzera,[41] T. LeCompte,[2] E. Lee,[51] H.S. Lee,[11] J.S. Lee,[25] S.W. Lee[w],[51] S. Leo[bb],[44] S. Leone,[44] J.D. Lewis,[15] C.-J. Lin,[26] J. Linacre,[40] M. Lindgren,[15] E. Lipeles,[43] A. Lister,[18] D.O. Litvintsev,[15] C. Liu,[45] Q. Liu,[46] T. Liu,[15] S. Lockwitz,[59] N.S. Lockyer,[43] A. Loginov,[59] D. Lucchesi[aa],[41] J. Lueck,[24] P. Lujan,[26] P. Lukens,[15] G. Lungu,[48] J. Lys,[26] R. Lysak,[12] R. Madrak,[15] K. Maeshima,[15] K. Makhoul,[30] P. Maksimovic,[23] S. Malik,[48] G. Manca[b],[27] A. Manousakis-Katsikakis,[3] F. Margaroli,[46] C. Marino,[24] M. Martínez,[4] R. Martínez-Ballarín,[29] P. Mastrandrea,[49] M. Mathis,[23] M.E. Mattson,[57] P. Mazzanti,[6] K.S. McFarland,[47] P. McIntyre,[51] R. McNulty[i],[27] A. Mehta,[27] P. Mehtala,[21] A. Menzione,[44] C. Mesropian,[48] T. Miao,[15] D. Mietlicki,[32] A. Mitra,[1] H. Miyake,[53] S. Moed,[20] N. Moggi,[6] M.N. Mondragon[k],[15] C.S. Moon,[25] R. Moore,[15] M.J. Morello,[15] J. Morlock,[24] P. Movilla Fernandez,[15] A. Mukherjee,[15] Th. Muller,[24] P. Murat,[15] M. Mussini[z],[6] J. Nachtman[m],[15] Y. Nagai,[53] J. Naganoma,[56] I. Nakano,[38] A. Napier,[54] J. Nett,[51] C. Neu,[55] M.S. Neubauer,[22] J. Nielsen[e],[26] L. Nodulman,[2] O. Norniella,[22] E. Nurse,[28] L. Oakes,[40] S.H. Oh,[14] Y.D. Oh,[25] I. Oksuzian,[55] T. Okusawa,[39] R. Orava,[21] L. Ortolan,[4] S. Pagan Griso[aa],[41] C. Pagliarone,[52] E. Palencia[f],[9] V. Papadimitriou,[15] A.A. Paramonov,[2] J. Patrick,[15] G. Pauletta[ff],[52] M. Paulini,[10] C. Paus,[30] D.E. Pellett,[7] A. Penzo,[52] T.J. Phillips,[14] G. Piacentino,[44] E. Pianori,[43] J. Pilot,[37] K. Pitts,[22] C. Plager,[8] L. Pondrom,[58] K. Potamianos,[46] O. Poukhov,[13] F. Prokoshin[x],[13] A. Pronko,[15] F. Ptohos[h],[17] E. Pueschel,[10] G. Punzi[bb],[44] J. Pursley,[58] A. Rahaman,[45] V. Ramakrishnan,[58] N. Ranjan,[46] I. Redondo,[29] P. Renton,[40] M. Rescigno,[49] F. Rimondi[z],[6] L. Ristori[45],[15] A. Robson,[19] T. Rodrigo,[9] T. Rodriguez,[43] E. Rogers,[22] S. Rolli,[54] R. Roser,[15] M. Rossi,[52] F. Rubbo,[15] F. Ruffini[cc],[44] A. Ruiz,[9] J. Russ,[10] V. Rusu,[15] A. Safonov,[51] W.K. Sakumoto,[47] Y. Sakurai,[56] L. Santi[ff],[52] L. Sartori,[44]

K. Sato,[53] V. Saveliev[t],[42] A. Savoy-Navarro,[42] P. Schlabach,[15] A. Schmidt,[24] E.E. Schmidt,[15] M.P. Schmidt,[59] M. Schmitt,[36] T. Schwarz,[7] L. Scodellaro,[9] A. Scribano[cc],[44] F. Scuri,[44] A. Sedov,[46] S. Seidel,[35] Y. Seiya,[39] A. Semenov,[13] F. Sforza[bb],[44] S. Sfyrla,[22] S.Z. Shalhout,[7] T. Shears,[27] P.F. Shepard,[45] M. Shimojima[s],[53] S. Shiraishi,[11] M. Shochet,[11] I. Shreyber,[34] A. Simonenko,[13] P. Sinervo,[31] A. Sissakian,[13] K. Sliwa,[54] J.R. Smith,[7] F.D. Snider,[15] A. Soha,[15] S. Somalwar,[50] V. Sorin,[4] P. Squillacioti,[15] M. Stancari,[15] M. Stanitzki,[59] R. St. Denis,[19] B. Stelzer,[31] O. Stelzer-Chilton,[31] D. Stentz,[36] J. Strologas,[35] G.L. Strycker,[32] Y. Sudo,[53] A. Sukhanov,[16] I. Suslov,[13] K. Takemasa,[53] Y. Takeuchi,[53] J. Tang,[11] M. Tecchio,[32] P.K. Teng,[1] J. Thom[g],[15] J. Thome,[10] G.A. Thompson,[22] E. Thomson,[43] P. Ttito-Guzmán,[29] S. Tkaczyk,[15] D. Toback,[51] S. Tokar,[12] K. Tollefson,[33] T. Tomura,[53] D. Tonelli,[15] S. Torre,[17] D. Torretta,[15] P. Totaro[ff],[52] M. Trovato[dd],[44] Y. Tu,[43] F. Ukegawa,[53] S. Uozumi,[25] A. Varganov,[32] F. Vázquez[k],[16] G. Velev,[15] C. Vellidis,[3] M. Vidal,[29] I. Vila,[9] R. Vilar,[9] J. Vizán,[9] M. Vogel,[35] G. Volpi[bb],[44] P. Wagner,[43] R.L. Wagner,[15] T. Wakisaka,[39] R. Wallny,[8] S.M. Wang,[1] A. Warburton,[31] D. Waters,[28] M. Weinberger,[51] W.C. Wester III,[15] B. Whitehouse,[54] D. Whiteson[c],[43] A.B. Wicklund,[2] E. Wicklund,[15] S. Wilbur,[11] F. Wick,[24] H.H. Williams,[43] J.S. Wilson,[37] P. Wilson,[15] B.L. Winer,[37] P. Wittich[g],[15] S. Wolbers,[15] H. Wolfe,[37] T. Wright,[32] X. Wu,[18] Z. Wu,[5] K. Yamamoto,[39] J. Yamaoka,[14] T. Yang,[15] U.K. Yang[p],[11] Y.C. Yang,[25] W.-M. Yao,[26] G.P. Yeh,[15] K. Yi[m],[15] J. Yoh,[15] K. Yorita,[56] T. Yoshida[j],[39] G.B. Yu,[14] I. Yu,[25] S.S. Yu,[15] J.C. Yun,[15] A. Zanetti,[52] Y. Zeng,[14] and S. Zucchelli[z][6]

(CDF Collaboration)

[1]*Institute of Physics, Academia Sinica, Taipei, Taiwan 11529, Republic of China*
[2]*Argonne National Laboratory, Argonne, Illinois 60439, USA*
[3]*University of Athens, 157 71 Athens, Greece*
[4]*Institut de Fisica d'Altes Energies, ICREA, Universitat Autonoma de Barcelona, E-08193, Bellaterra (Barcelona), Spain*
[5]*Baylor University, Waco, Texas 76798, USA*
[6]*Istituto Nazionale di Fisica Nucleare Bologna, [z]University of Bologna, I-40127 Bologna, Italy*
[7]*University of California, Davis, Davis, California 95616, USA*
[8]*University of California, Los Angeles, Los Angeles, California 90024, USA*
[9]*Instituto de Fisica de Cantabria, CSIC-University of Cantabria, 39005 Santander, Spain*
[10]*Carnegie Mellon University, Pittsburgh, Pennsylvania 15213, USA*
[11]*Enrico Fermi Institute, University of Chicago, Chicago, Illinois 60637, USA*
[12]*Comenius University, 842 48 Bratislava, Slovakia; Institute of Experimental Physics, 040 01 Kosice, Slovakia*
[13]*Joint Institute for Nuclear Research, RU-141980 Dubna, Russia*
[14]*Duke University, Durham, North Carolina 27708, USA*
[15]*Fermi National Accelerator Laboratory, Batavia, Illinois 60510, USA*
[16]*University of Florida, Gainesville, Florida 32611, USA*
[17]*Laboratori Nazionali di Frascati, Istituto Nazionale di Fisica Nucleare, I-00044 Frascati, Italy*
[18]*University of Geneva, CH-1211 Geneva 4, Switzerland*
[19]*Glasgow University, Glasgow G12 8QQ, United Kingdom*
[20]*Harvard University, Cambridge, Massachusetts 02138, USA*
[21]*Division of High Energy Physics, Department of Physics, University of Helsinki and Helsinki Institute of Physics, FIN-00014, Helsinki, Finland*
[22]*University of Illinois, Urbana, Illinois 61801, USA*
[23]*The Johns Hopkins University, Baltimore, Maryland 21218, USA*
[24]*Institut für Experimentelle Kernphysik, Karlsruhe Institute of Technology, D-76131 Karlsruhe, Germany*
[25]*Center for High Energy Physics: Kyungpook National University, Daegu 702-701, Korea; Seoul National University, Seoul 151-742, Korea; Sungkyunkwan University, Suwon 440-746, Korea; Korea Institute of Science and Technology Information, Daejeon 305-806, Korea; Chonnam National University, Gwangju 500-757, Korea; Chonbuk National University, Jeonju 561-756, Korea*
[26]*Ernest Orlando Lawrence Berkeley National Laboratory, Berkeley, California 94720, USA*
[27]*University of Liverpool, Liverpool L69 7ZE, United Kingdom*
[28]*University College London, London WC1E 6BT, United Kingdom*
[29]*Centro de Investigaciones Energeticas Medioambientales y Tecnologicas, E-28040 Madrid, Spain*
[30]*Massachusetts Institute of Technology, Cambridge, Massachusetts 02139, USA*
[31]*Institute of Particle Physics: McGill University, Montréal, Québec, Canada H3A 2T8; Simon Fraser University, Burnaby, British Columbia, Canada V5A 1S6; University of Toronto, Toronto, Ontario, Canada M5S 1A7; and TRIUMF, Vancouver, British Columbia, Canada V6T 2A3*
[32]*University of Michigan, Ann Arbor, Michigan 48109, USA*
[33]*Michigan State University, East Lansing, Michigan 48824, USA*
[34]*Institution for Theoretical and Experimental Physics, ITEP, Moscow 117259, Russia*

[35] *University of New Mexico, Albuquerque, New Mexico 87131, USA*
[36] *Northwestern University, Evanston, Illinois 60208, USA*
[37] *The Ohio State University, Columbus, Ohio 43210, USA*
[38] *Okayama University, Okayama 700-8530, Japan*
[39] *Osaka City University, Osaka 588, Japan*
[40] *University of Oxford, Oxford OX1 3RH, United Kingdom*
[41] *Istituto Nazionale di Fisica Nucleare, Sezione di Padova-Trento,* [aa] *University of Padova, I-35131 Padova, Italy*
[42] *LPNHE, Universite Pierre et Marie Curie/IN2P3-CNRS, UMR7585, Paris, F-75252 France*
[43] *University of Pennsylvania, Philadelphia, Pennsylvania 19104, USA*
[44] *Istituto Nazionale di Fisica Nucleare Pisa,* [bb] *University of Pisa,*
[cc] *University of Siena and* [dd] *Scuola Normale Superiore, I-56127 Pisa, Italy*
[45] *University of Pittsburgh, Pittsburgh, Pennsylvania 15260, USA*
[46] *Purdue University, West Lafayette, Indiana 47907, USA*
[47] *University of Rochester, Rochester, New York 14627, USA*
[48] *The Rockefeller University, New York, New York 10065, USA*
[49] *Istituto Nazionale di Fisica Nucleare, Sezione di Roma 1,*
[ee] *Sapienza Università di Roma, I-00185 Roma, Italy*
[50] *Rutgers University, Piscataway, New Jersey 08855, USA*
[51] *Texas A&M University, College Station, Texas 77843, USA*
[52] *Istituto Nazionale di Fisica Nucleare Trieste/Udine,*
I-34100 Trieste, [ff] *University of Trieste/Udine, I-33100 Udine, Italy*
[53] *University of Tsukuba, Tsukuba, Ibaraki 305, Japan*
[54] *Tufts University, Medford, Massachusetts 02155, USA*
[55] *University of Virginia, Charlottesville, VA 22906, USA*
[56] *Waseda University, Tokyo 169, Japan*
[57] *Wayne State University, Detroit, Michigan 48201, USA*
[58] *University of Wisconsin, Madison, Wisconsin 53706, USA*
[59] *Yale University, New Haven, Connecticut 06520, USA*
(Dated: May 17, 2011)

We report on a search for the production of the Higgs boson decaying to two bottom quarks accompanied by two additional quarks. The data sample used corresponds to an integrated luminosity of approximately $4\,\mathrm{fb}^{-1}$ of $p\bar{p}$ collisions at $\sqrt{s} = 1.96\,\mathrm{TeV}$ recorded by the CDF II experiment. This search includes twice the integrated luminosity of the previous published result, uses new analysis techniques to distinguish jets originating from light flavor quarks and those from gluon radiation, and adds sensitivity to a Higgs boson produced by vector boson fusion. We find no evidence of the Higgs boson and place limits on the Higgs boson production cross-section for Higgs boson masses between $100\,\mathrm{GeV}/c^2$ and $150\,\mathrm{GeV}/c^2$ at the 95% confidence level. For a Higgs boson mass of $120\,\mathrm{GeV}/c^2$ the observed (expected) limit is 10.5 (20.0) times the predicted Standard Model cross-section.

I. INTRODUCTION

The Higgs boson remains the only undiscovered particle of the standard model (SM) of particle physics. It is the physical manifestation of the mechanism which provides mass to fundamental particles [1, 2]. Direct searches at the LEP collider have excluded a Higgs boson mass $m_H < 114.4\,\mathrm{GeV}/c^2$ at 95% confidence level (CL) [3], while the Tevatron has excluded a Higgs boson mass between $163\,\mathrm{GeV}/c^2$ and $166\,\mathrm{GeV}/c^2$ at 95% CL [4]. The Tevatron has reported a preliminary update which extends the exclusion region for a Higgs boson mass between 158 and $173\,\mathrm{GeV}/c^2$ [5]. Global fits to precision electroweak measurements set a one-sided 95% CL upper limit on m_H at $157\,\mathrm{GeV}/c^2$ [6].

This paper presents the results of a search for the Higgs boson using an integrated luminosity of $4\,\mathrm{fb}^{-1}$ of $p\bar{p}$ collision data at $\sqrt{s} = 1.96\,\mathrm{TeV}$ recorded by the Collider Detector at Fermilab (CDF II). We search for a Higgs boson decaying to a pair of bottom-quark jets ($b\bar{b}$) accompanied by two additional quark jets (qq') for Higgs

mass $100 \leq m_H \leq 150\,\mathrm{GeV}/c^2$. This search is most sensitive to a Higgs boson with low mass, $m_H < 135\,\mathrm{GeV}/c^2$, where the Higgs boson decay to $b\bar{b}$ is dominant [7]. The two production channels studied are associated production and vector boson fusion (VBF). The associated production channel is $p\bar{p} \to VH \to qq' b\bar{b}$, where V is a W/Z vector boson, which decays to a pair of quarks. The hadronic branching fraction of V to qq' is $\simeq 70\%$ [8]. In the VBF channel, $p\bar{p} \to qq'H \to qq' b\bar{b}$, the incoming partons each radiate a V and the two V fuse to form a Higgs boson.

Low-mass Higgs boson searches at CDF have concentrated on signatures that are a combination of jets, leptons and missing transverse energy which help to reduce the backgrounds but the signal yields are small [9–11]. The hadronic modes used in this search exploit the larger branching fraction and thus have the largest signal yields among all the search channels at CDF. The major challenge for this search is the modeling and suppression of the large background from QCD multijets (referred to as QCD for brevity).

A previous paper on the search for the Higgs boson in the all-hadronic channel was published using an integrated luminosity of $2\,\mathrm{fb}^{-1}$ [12]. This paper has lowered the expected limit by a factor of two: a factor of $\approx \sqrt{2}$ from doubling the analyzed data and a factor of 1.4 from improvements to the analysis which are discussed in this paper.

II. THE TEVATRON AND THE CDF II DETECTOR

The CDF II detector is an azimuthally and forward-backward symmetric detector designed to study $p\bar{p}$ collisions and is described in detail in Refs. [13–15] and references therein. CDF II uses a cylindrical coordinate system with the z axis aligned along the proton beam direction, θ is the polar angle relative to the z-axis and ϕ is the azimuthal angle relative to the x-axis. The pseudo-rapidity is defined as $\eta \equiv -\ln(\tan\theta/2)$. The transverse energy is $E_T \equiv E\sin\theta$. Jets are defined by a cluster of energy in the calorimeter deposited inside a cone of radius $\Delta R = \sqrt{(\Delta\phi)^2 + (\Delta\eta)^2} = 0.4$ as reconstructed by the JetClu algorithm [16]. Corrections are applied to the measured jet energy to account for detector calibrations, multiple interactions, underlying event and energy outside of the jet cone [17].

The data for this search were collected by two multijet triggers. The first $2.8\,\mathrm{fb}^{-1}$ used a trigger which selected at least four jet clusters with $E_T \geq 15\,\mathrm{GeV}$ and total $E_T \geq 175\,\mathrm{GeV}$. This trigger was used in the previous result [12]. The remaining $1.1\,\mathrm{fb}^{-1}$ were recorded with a new trigger which selected at least three jet clusters with $E_T \geq 20\,\mathrm{GeV}$ and total $E_T \geq 130\,\mathrm{GeV}$. The new trigger improves the acceptance for low-mass Higgs boson from 20% to 45%.

III. EVENT SELECTION

Events with isolated leptons or missing transverse energy significance [18] > 6 are removed to avoid any overlap with other low mass Higgs analyses at CDF II. The data are refined further by selecting events with four or five jets where each jet has $E_T > 15\,\mathrm{GeV}$ and $|\eta| < 2.4$. The selected jets are ordered by descending jet-E_T and any fifth jet plays no further role. The scalar sum of the four leading jets' E_T is required to be $> 220\,\mathrm{GeV}$, and exactly two of the four leading jets are required to be identified ("tagged") as bottom-quark jets (b jet). A b jet is identified by its displaced vertex, as defined by the SecVtx algorithm [14], or by using the probability that the tracks within the jet are inconsistent with originating from the primary $p\bar{p}$ collision as defined by the JetProb algorithm [19]. The final four jets are labeled as b_1, b_2, q_1, q_2 where $b(q)$ are tagged (untagged) jets and $b_1(q_1)\,E_T > b_2(q_2)\,E_T$.
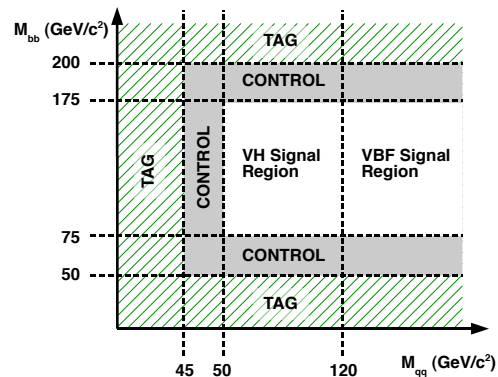

FIG. 1: $m_{bb} - m_{qq}$ plane: This plane illustrates the VH and VBF signal regions used to select VH and VBF candidates. The Tag region is used to derive a model of the QCD background. The Control region measures the systematic uncertainty of the QCD model.

The signal/background ratio is enhanced by dividing the data into two non-overlapping b-tagging categories: SS when both jets are tagged by SecVtx, SJ when one jet is tagged by SecVtx and the other by JetProb. For a jet tagged by both algorithms, SecVtx takes precedence as it has a lower rate of misidentifying a light flavor jet as a b jet. The previous $2\,\mathrm{fb}^{-1}$ search only included the SS category [12] and the addition of the SJ category increases the signal acceptance by 36%. Other b-tagging combinations, such as both b jets selected by JetProb, were not considered in this search as the relative increase in the background is much larger than that for the signal.

The data are divided into VH and VBF candidates defined by the invariant masses of the $b_1 b_2$ pair, m_{bb}, and the $q_1 q_2$ pair, m_{qq}. VH candidates have $75 < m_{bb} < 175\,\mathrm{GeV}/c^2$ and $50 < m_{qq} < 120\,\mathrm{GeV}/c^2$. VBF candidates have $75 < m_{bb} < 175\,\mathrm{GeV}/c^2$ and $m_{qq} > 120\,\mathrm{GeV}/c^2$. The typical m_{bb} dijet mass resolution is $\sim 18\%$ [11]. These VH and VBF signal regions are illustrated in Fig. 1. We search for Higgs bosons produced via VH and VBF exclusively in the VH and VBF signal regions respectively. The division of events is based on the different kinematics of the two processes. The VH channel has two mass resonances: m_{bb} from the Higgs boson decay and m_{qq} from the V decay. The VBF channel shares the same m_{bb} Higgs boson mass resonance but there is no accompanying resonance for m_{qq}. The q jets in VBF tend to have a large η separation which results in larger values of m_{qq}. The cut of $m_{qq} > 120\,\mathrm{GeV}/c^2$ optimizes the VBF signal over background ratio. The acceptance for VH and VBF events varies from 2% to 3% for $100\,\mathrm{GeV}/c^2 < m_H < 150\,\mathrm{GeV}/c^2$. As VH and VBF candidates are also split by the two b-tagging categories, there are 4 independent samples (channels) which are studied: VH-SS; VH-SJ; VBF-SS; VBF-SJ.

TABLE I: Expected number of non-QCD background and VH/VBF signal with observed number of events for the four channels. Statistical and systematic uncertainties are combined in quadrature where systematic uncertainties dominate. The number of VH(VBF) events are exclusive to the VH(VBF) channels. The difference between data and non-QCD are assumed to be QCD.

	VH-SS	VH-SJ	VBF-SS	VBF-SJ
$t\bar{t}$	281.7 ± 45.6	115.3 ± 19.9	177.3 ± 28.7	75.7 ± 13.1
Single-top	44.1 ± 7.1	17.7 ± 3.1	17.2 ± 2.8	10.0 ± 1.7
Z + Jets	127.5 ± 65.8	55.4 ± 28.8	135.0 ± 69.7	62.9 ± 32.7
W + HF	27.9 ± 14.4	12.0 ± 6.2	4.8 ± 2.5	3.3 ± 1.7
Diboson	11.4 ± 1.6	8.5 ± 1.3	5.3 ± 0.7	3.8 ± 0.6
Total Non-QCD	492.6 ± 81.7	208.9 ± 35.7	339.6 ± 75.5	155.7 ± 35.3
Higgs Signal ($m_H = 120\,\text{GeV}/c^2$)				
VH	7.8 ± 1.0	2.9 ± 0.4		
VBF			3.2 ± 0.4	1.2 ± 0.2
Data	16857	9341	17776	9518

IV. SIGNAL AND BACKGROUND SAMPLES

The data are compared to a model of the signal and background composed of QCD, $t\bar{t}$, $Z(\to b\bar{b}/c\bar{c})$ + Jets (Z+jets), single-top, $W + b\bar{b}/c\bar{c}$ (W+HF), and $WW/WZ/ZZ$ (diboson) events. The signal and non-QCD backgrounds are modeled by Monte Carlo (MC) simulation. The VH and VBF production are generated by PYTHIA [20] and combined with a GEANT-based [21] simulation of the CDF II detector [22]. The non-QCD MC is described in detail in Ref. [12] and normalized to next-to-leading order cross sections. All the MC samples include the trigger simulation and their trigger efficiencies are corrected as described in Ref. [12]. The QCD background shape is modeled by a data-driven technique developed in Ref. [12] and described in detail below. The expected signal yields of the four channels are 7.8(VH-SS), 2.9(VH-SJ), 3.2(VBF-SS), and 1.2(VBF-SJ) for $m_H = 120\,\text{GeV}/c^2$. The total backgrounds are about 17000(VH-SS), 9300(VH-SJ), 18000(VBF-SS), and 9500(VBF-SJ). The background composition is $\sim$98% QCD (Table I).

V. QCD MODELING

The dominant QCD background shape is modeled using a data-driven method known as the tag rate function (TRF) and described in detail in [12]. The TRF is applied to a QCD dominated data sample of events with at least one SECVTX b-tagged jet (single-tagged events) to predict the distribution of events with exactly two b-tagged jets (double-tagged events). For each single-tagged event, the TRF gives the probability of each additional jet, called a *probe* jet, to be a second b-tagged jet. The TRF is parameterized as a function of three variables: the probe jet-E_T, probe jet-η and ΔR between the

tagged b jet and probe jet. The choice of variables used to parameterize the TRF is motivated by the kinematics of QCD and the characteristics of the b-tagging algorithms. As the behavior of the SECVTX and JETPROB b-tagging algorithms are not identical, there is a TRF for SS and another TRF for SJ. The TRF is measured using jets in the TAG region (Fig. 1), defined as $m_{qq} < 45\,\text{GeV}/c^2$, $m_{bb} < 50\,\text{GeV}/c^2$ and $m_{bb} > 200\,\text{GeV}/c^2$ which is not in the VH and VBF signal regions.

VI. JET MOMENT

The VH and VBF q-jets are mostly quark jets while QCD q-jets are a mixture of gluon and quark jets. As gluon jets, on average, tend to be broader than quark jets, any variable related to the jet width is an additional tool to discriminate the Higgs signal from QCD.

In this paper, we introduce the jet $\phi(\eta)$ moment, $\langle\phi\rangle$ ($\langle\eta\rangle$), of q jets which measures the jet width along the $\phi(\eta)$ axis. The jet ϕ and η moments are defined by Eq.(1)

$$\langle\phi\rangle = \sqrt{\sum_{\text{towers}} \left[\frac{E_t^{\text{tower}}}{E_t^{\text{jet}}} \left(\Delta\phi(\phi_{\text{tower}}, \phi_{\text{jet}}) \right)^2 \right]} \quad (1\text{a})$$

$$\langle\eta\rangle = \sqrt{\sum_{\text{towers}} \left[\frac{E_t^{\text{tower}}}{E_t^{\text{jet}}} \left(\eta_{\text{tower}} - \eta_{\text{jet}} \right)^2 \right]} \quad (1\text{b})$$

where the summation for the jet moment is over the calorimeter towers used to form the jets and uses the tower-E_T (E_t^{tower}), the jet-E_T (E_t^{jet}), the tower's $\phi(\eta)$ position, ϕ_{tower} (η_{tower}), and the jet's $\phi(\eta)$ position, $\phi_{\text{jet}}(\eta_{\text{jet}})$. The function $\Delta\phi(\phi_{\text{tower}}, \phi_{\text{jet}})$ in Eq. 1a is the smallest angular difference between ϕ_{tower} and ϕ_{jet}. The jet moment is a measure of the jet's width.

We checked whether the MC simulation of the quark jet moment matches the data. Gluon jet moments were not checked as the Higgs q-jet, modelled by MC, are mostly quark jets whereas gluon jets only appear in QCD which is derived from data. The hadronic W decay from $t\bar{t} \to bW\bar{b}W \to bl\nu + \bar{b}qq'$, where l is an electron or muon, provides a source of quark jets. The event selection from Ref. [23] was used to extract a $t\bar{t}$ data sample which is 86% $t\bar{t}$. The complete sample composition is described in Ref. [23]. The leading untagged jet pair whose invariant mass is $80 \pm 30\,\text{GeV}/c^2$ are assumed to be the quark jets from the hadronic W boson decay. The same event and leading untagged jet pair selection is applied to $t\bar{t}$ MC to compare with data.

The jet moment depends not only on the parton initiating the jet but also on the jet-Et, jet-η and the number of primary vertices in the event (NVtx) which are not guaranteed to be the same for data and MC. The dependencies are removed by rescaling the measured jet moment to a common reference of jet-E_T=50 GeV/c^2, jet-η=0 and

NVtx=1, as measured in data. Eq. 2 demonstrates the rescaling for $\langle\phi\rangle$

$$\langle\phi\rangle'_{Data} = \langle\phi\rangle_{Data} \quad \times$$
$$\frac{f^{\phi}_{Data}(\text{Jet-}E_T=50\text{GeV}/c^2,\text{Jet-}\eta=0,\text{NVtx}=1)}{f^{\phi}_{Data}(\text{Jet-}E_T,\text{Jet-}\eta,\text{NVtx})} \quad (2a)$$

$$\langle\phi\rangle'_{MC} = \langle\phi\rangle_{MC} \quad \times$$
$$\frac{f^{\phi}_{Data}(\text{Jet-}E_T=50\text{GeV}/c^2,\text{Jet-}\eta=0,\text{NVtx}=1)}{f^{\phi}_{MC}(\text{Jet-}E_T,\text{Jet-}\eta,\text{NVtx})} \quad (2b)$$

where f^{ϕ}_{Data} (Jet-E_T, Jet-η, NVtx) and f^{ϕ}_{MC} (Jet-E_T, Jet-η, NVtx) are the $\langle\phi\rangle$ parameterizations for data and MC respectively. $\langle\phi\rangle_{Data}(\langle\phi\rangle_{MC})$ are the measured $\langle\phi\rangle$ for data(MC), and $\langle\phi\rangle'_{Data}(\langle\phi\rangle'_{MC})$ are the rescaled values. $\langle\eta\rangle$ is rescaled in a similar way but has a separate $\langle\eta\rangle$ parameterization for data and MC.

After rescaling the measured jet moments, the MC required an additional shift of $\sim +2\%$ to make it agree with the data. Half of this offset was used as an estimate of the systematic uncertainty of the MC jet moment. Figure 2 compares the jet moments of data to the simulated $t\bar{t}$ signal and background MC which are in the same fractions as measured in data. Only after applying all corrections does the MC agree with the data.

As an additional check, the $\langle\phi\rangle'_{MC}$ and $\langle\eta\rangle'_{MC}$ of $t\bar{t}$ MC were compared with VH and VBF MC. The average jet moments of the MC samples should be identical as the q-jets from $t\bar{t}$ and Higgs signal are just quark jets. For the VH sample, the jet moments agreed with $t\bar{t}$. However there was disagreement of 5% for VBF MC with $t\bar{t}$ MC for jets with $|\eta| > 1.1$. Half of this difference was used as an additional systematic error for the VBF jet moment.

VII. NEURAL NETWORK

The large background precludes the use of simple variables, such as m_{bb}, to search for a Higgs boson signal. An artificial neural network (NN), from the TMVA package [24], is trained to search exclusively for VH(VBF) Higgs bosons in the VH(VBF) signal region. The NN is trained using VH(VBF) signal and TRF QCD prediction as background. As the kinematics for VH and VBF Higgs signals are different, a dedicated NN for each signal is trained. The NN training variables for the VH NN are m_{bb}, m_{qq}, $q_1\langle\phi\rangle'$, $q_1\langle\eta\rangle'$, $q_2\langle\phi\rangle'$, $q_2\langle\eta\rangle'$, the cosine of the helicity angle $\cos\theta^*_{q_1}$ [25], the cosine of the leading jet scattering angle in the four jet rest frame, $\cos\theta_3$ [26] and χ which is a measure of whether both the b-jet pair and q-jet pair are from a Higgs boson and V decay respectively. χ is defined as the minimum of χ_W and χ_Z where χ_W is defined as $\chi_W = \sqrt{(M_W - M_{qq})^2 + (M_H - M_{bb})^2}$ and a similar expression exists for χ_Z. For the VBF channel, the neural net inputs are m_{bb}, m_{qq}, $q_1\langle\phi\rangle'$, $q_1\langle\eta\rangle'$, $q_2\langle\phi\rangle'$, and $q_2\langle\eta\rangle'$.

The two b-tagging categories have similar kinematic distributions which allows the same NN to be used for SS and SJ events. The NN is trained with SS events as it has the better signal/background ratio.

A. NN Training

Before training the NN, the TRF QCD modeling was verified by comparing the shapes of the NN training variables constructed from single-tagged events, after applying the TRF, and double tagged events from the TAG region. The TRF is able to reproduce the shapes of all the NN training variables except m_{qq} and the jet moments. The TRF is corrected using a correction function for each mismodeled variable. The correction function was constructed from the fitted ratio of the observed double tagged shape in the TAG region to the TRF prediction in the TAG region. The largest correction value was 2%. Figures 3 and 4 show distributions of the NN training variables of VH and VBF signal, corrected TRF QCD and double tagged data for the SS b-tagging category. The corrected TRF QCD follows the shape of the data for all variables. The TRF predictions for SJ were validated in the same way.

We search for a Higgs boson of mass $100 \leq m_H \leq 150\,\text{GeV}/c^2$ at $5\,\text{GeV}/c^2$ intervals. As m_{bb} is one of the NN training variables, which varies with different Higgs mass hypotheses, the Higgs search sensitivity can be improved by training the NN at different Higgs masses. There is a separate VH(VBF) NN trained at $m_H = 100\,\text{GeV}/c^2$, $120\,\text{GeV}/c^2$, and $140\,\text{GeV}/c^2$. For Higgs mass hypotheses between $100\,\text{GeV}/c^2$ and $110\,\text{GeV}/c^2$, the NN trained with $m_H = 100\,\text{GeV}/c^2$ is used. Similarly, we use the $m_H = 120\,\text{GeV}/c^2$ trained NN to search for a Higgs boson between $115\,\text{GeV}/c^2$ and $130\,\text{GeV}/c^2$ and the $m_H = 140\,\text{GeV}/c^2$ trained NN to search for a Higgs boson between $135\,\text{GeV}/c^2$ and $150\,\text{GeV}/c^2$.

Figure 5 shows the NN distributions for VH and VBF for a Higgs mass of $120\,\text{GeV}/c^2$. The NN returns a more negative (positive) score for background (signal) events. As the QCD background is large, QCD subtracted NN distributions are also shown.

VIII. SYSTEMATIC UNCERTAINTIES

We estimate the effect of systematic uncertainties by propagating uncertainties on the NN input variables to the NN output. We consider both variations on the normalization and shape of the NN output. The systematic uncertainties which affect the normalization of the Higgs signal and non-QCD backgrounds are: jet energy scale (JES) [17], parton distribution function (PDF), b-tagging scale factor between MC and data, initial and final state radiation (ISR/FSR), trigger efficiency, integrated luminosity and cross-sections [5]. The uncertain-
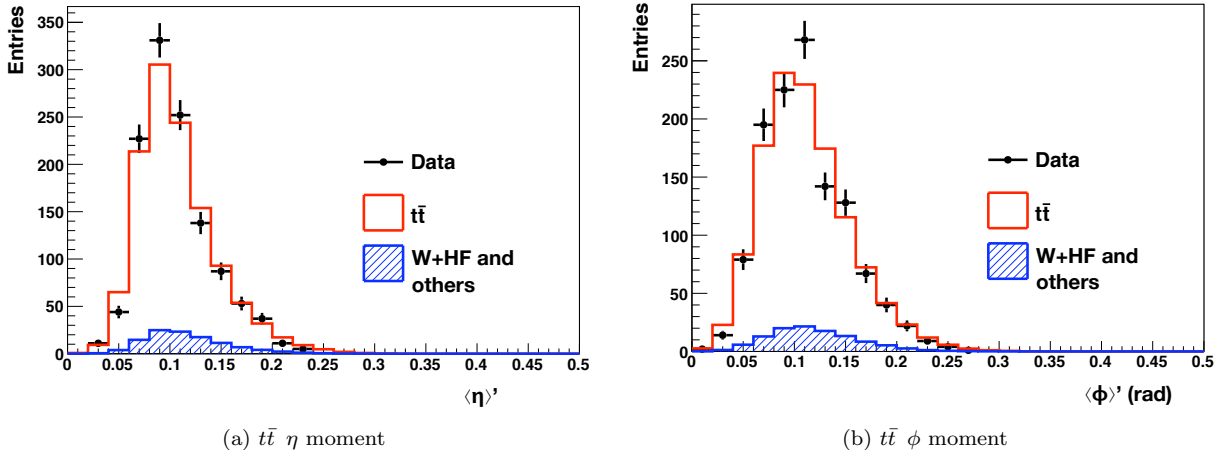
(a) $t\bar{t}$ η moment

(b) $t\bar{t}$ ϕ moment

FIG. 2: Comparisons of the jet moments of $t\bar{t}$ data to $t\bar{t}$ and W+HF, Z+jets, single top, disboson, misidentified b-jets (W+HF and others) MC. Only after applying all corrections does the MC agree with data.

ties which affect the shape of the NN output for the Higgs signal are the JES, ISR/FSR and jet moments. The uncertainties are summarized in table II.

For the TRF QCD prediction, we consider two shape uncertainties: an interpolation uncertainty and correction function uncertainty for m_{qq}, $\langle\phi\rangle$, and $\langle\eta\rangle$ variables. The interpolation uncertainty accounts for possible difference in the TRF between the regions where it was measured (TAG) and applied (SIGNAL) (Fig. 1). An alternative TRF was measured using events in the CONTROL region, as indicated in Fig. 1, which is still background-dominated. The interpolation uncertainty is defined as the difference of the QCD NN shapes using the nominal TAG TRF and CONTROL TRF. The correction function uncertainty for m_{qq} is evaluated by deriving an alternative correction function for m_{qq} using events from the CONTROL region. This alternative m_{qq} correction function is applied to the TRF, instead of the nominal m_{qq} correction function, and propagated through the NN. The difference in the QCD NN shape between using the nominal correction function and the CONTROL region derived function defines the correction function shape uncertainty. The systematic uncertainty for $\langle\phi\rangle$, and $\langle\eta\rangle$ correction functions is evaluated in the same way. The QCD NN output varied at most by $\sim 2 - 3\%$ for each QCD shape systematic.

IX. RESULTS

The NN output distribution of data are compared to the background and we find no excess of events over the expected background. We calculate upper limits on the excluded Higgs boson cross-section at the 95% CL for Higgs boson mass hypotheses $100 \leq m_H \leq 150 \, \mathrm{GeV}/c^2$ at $5 \, \mathrm{GeV}/c^2$ intervals. The limits are calculated using a Bayesian likelihood method with a flat prior for the signal

TABLE II: Summary of systematic uncertainties

Source	Uncertainty
Higgs and non-QCD uncertainties	
Integrated Luminosity	$\pm6\%$
Trigger efficiency	$\pm4\%$
PDF	$\pm2\%$
JES	$\pm7\%$ and shape
b-tagging scale factor	$\pm7.6\%$ for SS
	$\pm9.7\%$ for SJ
ISR/FSR	$\pm2\%$ and shape for VH
	$\pm3\%$ and shape for VBF
$\langle\phi\rangle'$ and $\langle\eta\rangle'$	shape for VH and VBF
$t\bar{t}$ and single-top cross section	$\pm10\%$
Diboson cross-section	$\pm6\%$
W+HF & Z+Jets cross-section	$\pm50\%$
QCD uncertainties	
interpolation	shape
m_{qq} correction function	shape
$\langle\phi\rangle$ correction function	shape
$\langle\eta\rangle$ correction function	shape

cross-section, integrating over Gaussian priors for the systematic uncertainties, incorporating correlated rate and shape uncertainties, and uncorrelated bin-by-bin statistical uncertainties [27]. The QCD normalization is a free parameter that is fit to the data.

The median of the 95% CL obtained from 10000 simulated experiments is taken at the expected 95% CL. The $\pm1\sigma$ (where σ denotes the standard deviation) and $\pm2\sigma$ expected limits are derived from the 16th, 84th, 2nd and 98th percentiles of the distribution, respectively.

For $m_H = 120 \, \mathrm{GeV}/c^2$, the observed (expected) limit, normalized to the SM cross-section, for the individual analysis channels are 11.9(25.6) for VH-SS, 43.4(51.8) for VH-SJ, 47.0(49.4) for VBF-SS, 93.7(132.3) for VBF-SJ, and 10.5(20.0) for the combination of these four channels. The combined channel limits for Higgs boson masses in the range between 100 - 150 GeV/c^2 are shown in Fig. 6 and summarized in Table III.

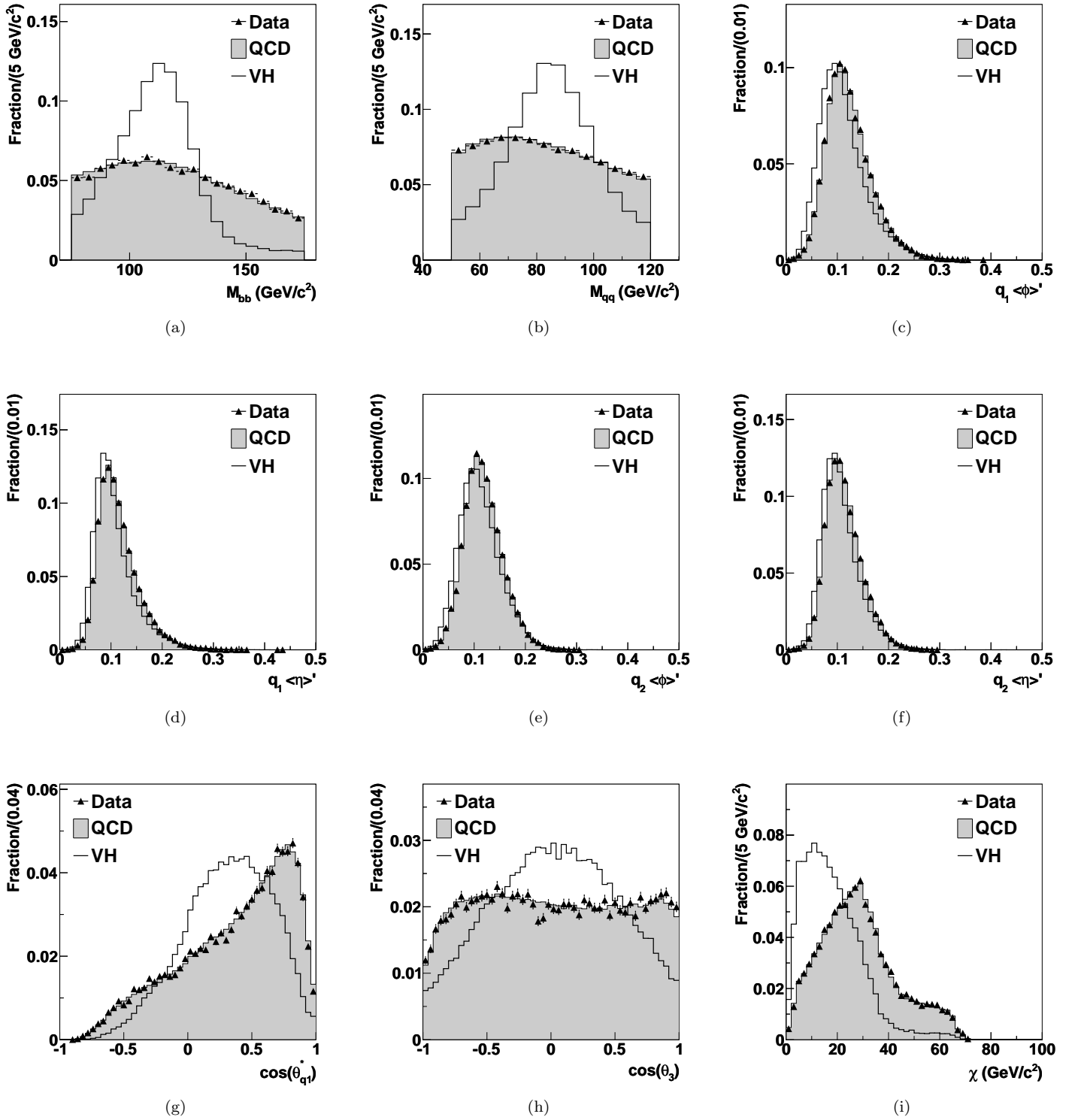The observed limits for the individual search channels

FIG. 3: Distribution of variables used to train the VH NN. The signal are VH ($m_H = 120\,\mathrm{GeV}/c^2$) SS events and the background are TRF predicted QCD SS events which have passed the VH candidate selection. All plots are normalised to unit area to compare shapes. After correction functions have been applied to m_{qq} and the jet-moments, the TRF correctly predicts the shape of the double-tagged SS data for all variables
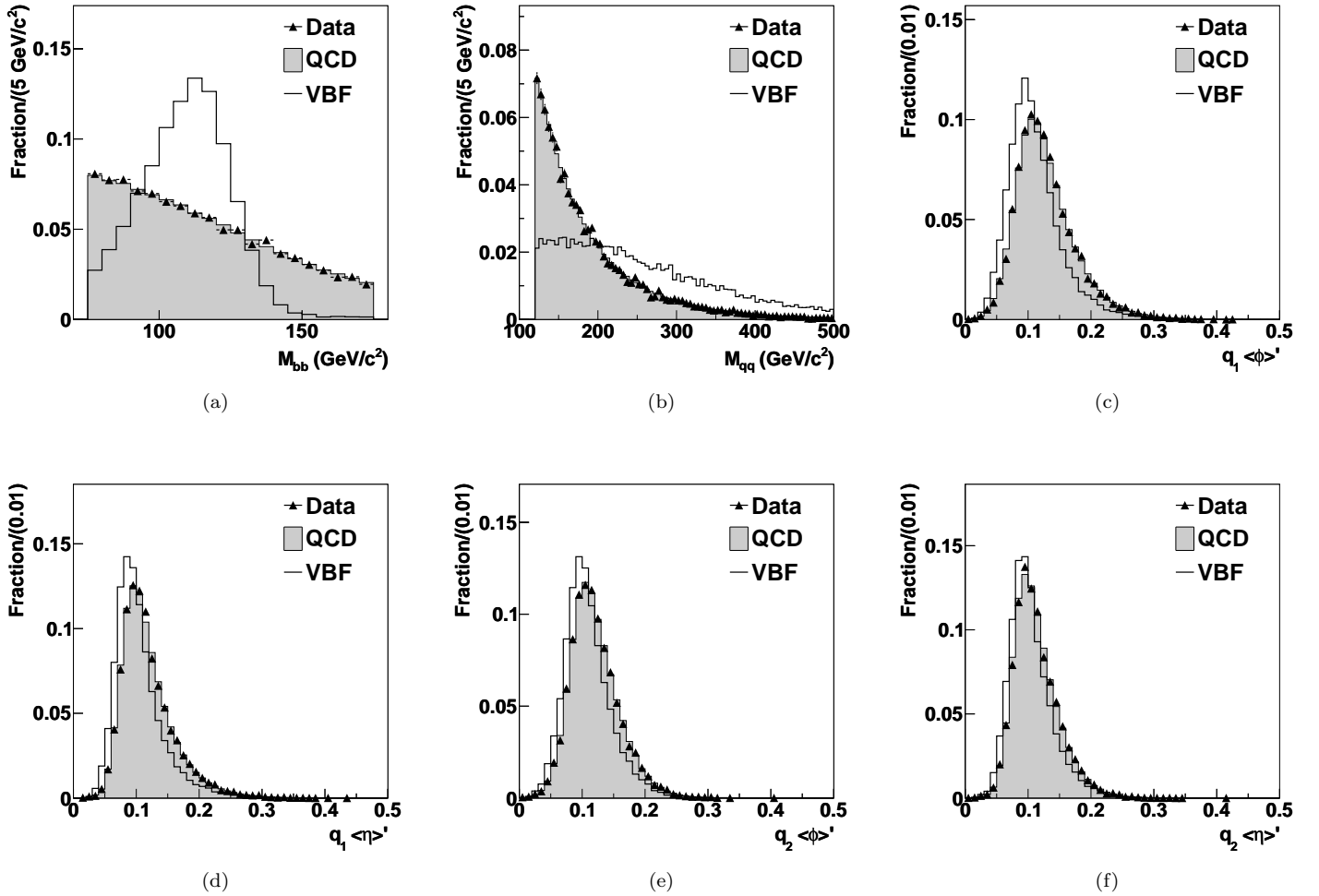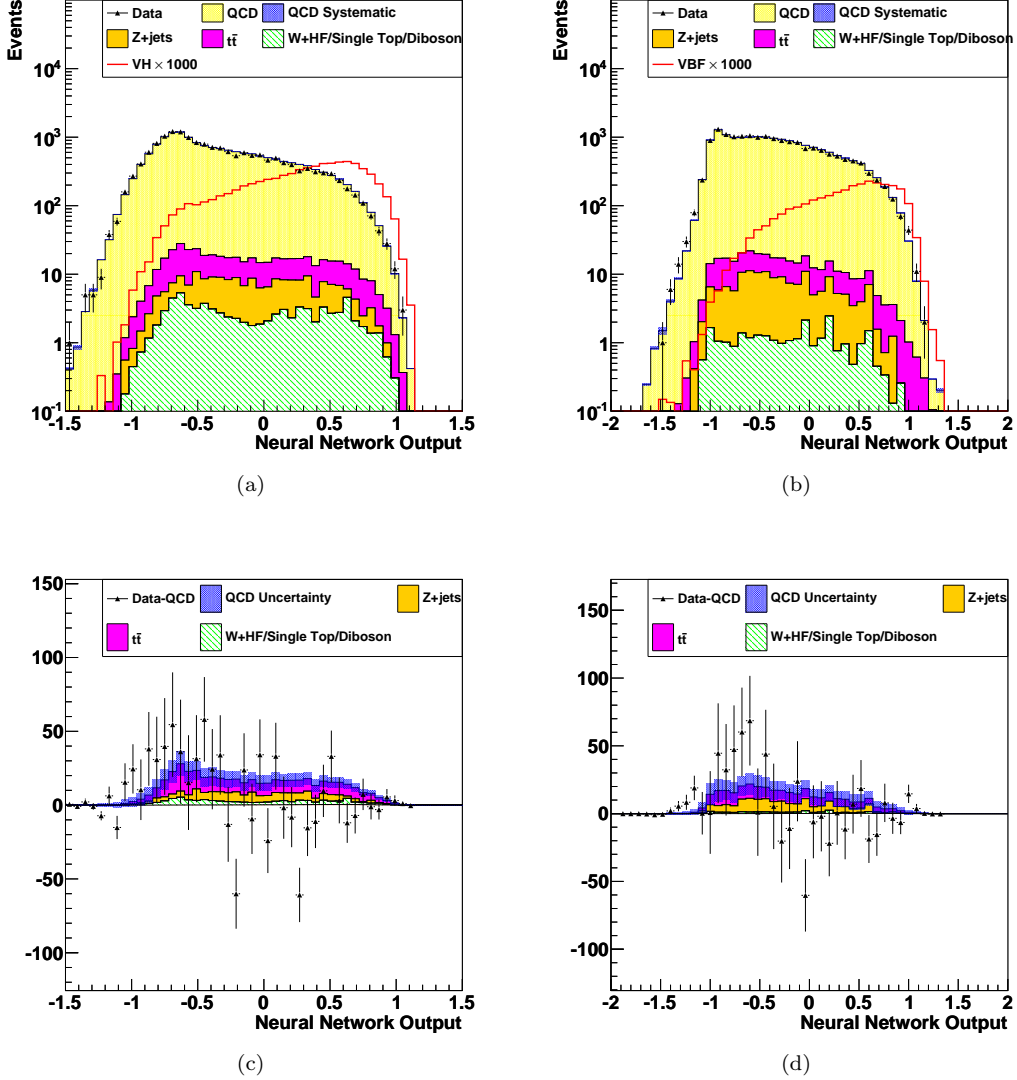
FIG. 4: Distribution of variables used to train the VBF NN. The signal are VBF ($m_H = 120 \, \text{GeV}/c^2$) SS events and the background are TRF predicted QCD SS events and which have passed the VBF candidate selection. All plots are normalised to unit area to compare shapes. After correction functions have been applied to m_{qq} and the jet-moments, the TRF correctly predicts the shape of the double-tagged SS data for all variables.

FIG. 5: NN distribution for VH-SS (a) and VBF-SS (b) for $m_H = 120\,\text{GeV}/c^2$. The VH and VBF distribution are scaled by a factor of 1000. As the QCD background is large, data-QCD versions are shown for VH (c) and VBF (d).

TABLE III: Expected and observed 95% CL upper limits for the combined VH and VBF channels. The limits are normalized to the expected Higgs cross-section.

Higgs mass (GeV/c^2)	-2σ	-1σ	Median	$+1\sigma$	$+2\sigma$	Observed
100	9.1	12.8	18.8	27.2	38.5	10.1
105	8.7	12.1	17.4	25.2	35.8	9.9
110	8.0	11.7	17.1	24.5	34.2	10.2
115	8.8	12.2	17.8	25.9	36.9	9.1
120	9.3	13.7	20.0	28.5	39.5	10.5
125	13.5	18.7	27.3	39.8	57.0	13.8
130	17.0	24.4	36.1	52.8	75.4	17.2
135	19.6	28.6	41.9	59.7	82.7	22.7
140	26.7	40.7	60.4	86.6	120.2	35.2
145	43.4	63.5	95.7	142.1	205.3	55.8
150	73.8	109.9	164.1	240.3	341.9	101.0

agree within 1σ of their expected limit except for the VH-SS channel where there is a 2σ difference. The observed data in the VH-SS channel has a deficit in the high signal region of the NN. As the VH-SS channel is the most sensitive, it has the strongest influence on the combined limit; thus the deviation of the observed limit from the expected limit in the VH-SS channel is similar to the combined limit. Figure 7 shows the ratio of the data to the expected background for the four analysis channels for the NN trained on a $120\,\text{GeV}/c^2$ Higgs boson. All four channels show a ratio ≈ 1 over the whole NN output range but the VH-SS channel has several points with a ratio of ≈ 0.9 at NN output of ~ 0.5; the high signal region of NN output. If the background is mismodeled, either the TRF has incorrectly predicted the
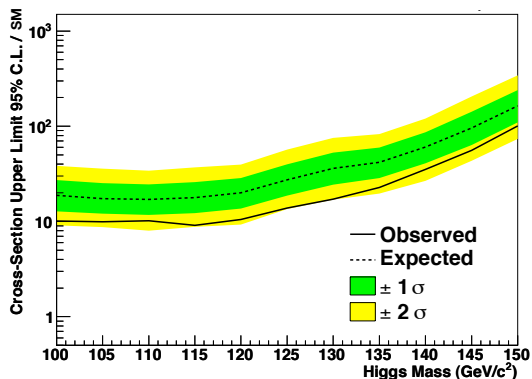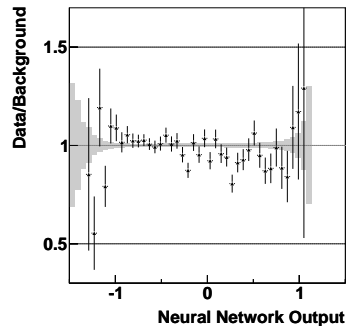
FIG. 6: Expected (dashed) and observed (solid) 95% CL normalized to the SM cross-section for the combined VH and VBF channel. The dark (light) band represents the $1\sigma(2\sigma)$ expected limit range.

QCD background or the NN is at fault. The VH-SS and VBF-SS channels share the same TRF and the VBF-SS observed limit agrees with its expected limit. The VH-SS and VH-SJ channel share the same trained NN and VH-SJ observed limit agrees with its expected limit. As neither the NN nor TRF appear to be at fault, it suggests the low ratio for VH-SS is likely to be a statistical fluctuation rather than evidence of background mismodeling.

X. SUMMARY

In summary, the measurement presented in this paper shows a factor of two improvement over the previous $2\,\mathrm{fb}^{-1}$ result for the all-hadronic Higgs search [12] . This paper extends the $2\,\mathrm{fb}^{-1}$ analysis by including the VBF channel, adding an additional algorithm to identify bottom-quark jets, adding an artificial neural network to separate signal from background which includes $\langle\phi\rangle$ and $\langle\eta\rangle$ to distinguish gluons from quark jets, and by doubling the analyzed data set. CDF II continues to collect more data and further improvements to the analysis technique will extend the sensitivity of the all-hadronic Higgs boson search.
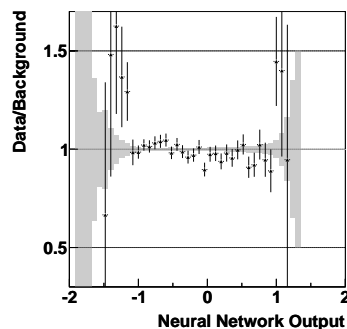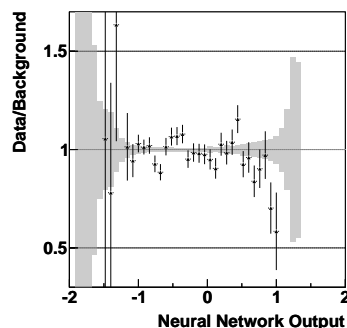
(a) VH-SS

(b) VH-SJ

(c) VBF-SS

(d) VBF-SJ

FIG. 7: Ratios of the data to background for VH-SS (a), VH-SJ (b), VBF-SS (c), and VBF-SJ (d) for the NN trained on $120\,\mathrm{GeV}/c^2$ Higgs boson MC. The error bars of the data to background ratio are the statistical errors. The solid gray band is the ratio of the background systematic uncertainty to the background.

[1] P. W. Higgs, Phys. Lett., **12**, 132 (1964).

[2] F. Englert, Phys. Rev. Lett., **13**, 321 (1964).

[3] The ALEPH, DELPHI, L3 and OPAL Collaborations, and the LEP Working Group for Higgs boson searches, Phys. Lett. B, **565**, 61 (2003).

[4] T. Aaltonen *et al.* (CDF Collaboration), Phys. Rev. Lett., **104**, 061802 (2010).

[5] CDF Collaboration and D0 Collaboration and Tevatron New Physics and Higgs Working Group, "Combined CDF and D0 upper limits on standard model higgs-boson production with up to $6.7\,\mathrm{fb}^{-1}$ of data," arXiv:hep-ex/1007.4587v1.

[6] ALEPH, CDF, D0, DELPHI, L3, OPAL, SLD, the LEP Electroweak Working Group, the Tevatron Electroweak Working Group, and the SLD Electroweak and Heavy Flavor Working Groups, "Precision Electroweak Measurements and Constraints on the Standard Model," arXiv:hep-ex/0911.2604.

[7] A. Djouadi, J. Kalinowski, and M. Spira, Comput. Phys. Commun., **108**, 56 (1998).

[8] C. Amsler *et al.*, Phys. Lett. B, **667**, 1 (2008).

[9] T. Aaltonen *et al.* (CDF Collaboration), Phys. Rev. D, **80**, 071101 (2009).

[10] T. Aaltonen *et al.* (CDF Collaboration), Phys. Rev. Lett., **103**, 101802 (2009).

[11] T. Aaltonen *et al.* (CDF Collaboration), Phys. Rev. Lett., **104**, 141801 (2010).

[12] T. Aaltonen *et al.* (CDF Collaboration), Phys. Rev. Lett., **103**, 221801 (2009).

[13] D. E. Acosta *et al.* (CDF Collaboration), Phys. Rev. D, **71**, 032001 (2005).

[14] D. E. Acosta *et al.* (CDF Collaboration), Phys. Rev. D, **71**, 052003 (2005).

[15] A. Abulencia *et al.* (CDF Collaboration), J. Phys. G, **34**, 2457 (2007).

[16] F. Abe *et al.* (CDF Collaboration), Phys. Rev. D, **45**, 1448 (1992).

[17] A. Bhatti *et al.* (CDF Collaboration), Nucl. Instrum. Methods, **A566**, 375 (2006).

[18] Missing transverse energy significance is defined as the ratio of the total missing transverse energy to the square root of the total transverse energy.

[19] A. Abulencia *et al.* (CDF Collaboration), Phys. Rev. D, **74**, 072006 (2006).

[20] T. Sjostrand *et al.*, Comput. Phys. Commun., **135**, 238 (2001).

[21] R. Brun *et al.*, CERN-DD-EE-84-01 (1987).

[22] E. Gerchtein and M. Paulini, arXiv:hep-ex/0306031.

[23] T. Aaltonen *et al.* (CDF Collaboration), Phys. Rev. Lett., **105**, 012001 (2010).

[24] A. Hoecker *et al.*, arXiv:hep-ex/0703039v5.

[25] $\cos\theta_{q_1}^*$ is the cosine helicity angle of q_1. The q_1 helicity angle, $\theta_{q_1}^*$, is defined to be the angle between the momentum of q_1 in the $q_1 - q_2$ rest frame and the total momentum of $q_1 - q_2$ in the lab frame.

[26] $\cos\theta_3$ is defined in a three jet rest frame as the cosine of the leading jet scattering angle. We reduce from four jets to three jets by combining the two jets with the lowest dijet mass. Thus $\cos\theta_3 = \frac{\vec{P_{AV}}\cdot\vec{P_3}}{|\vec{P_{AV}}||\vec{P_3}|}$, where $\vec{P_3}$ is the third jet and $\vec{P_{AV}}$ is the vector sum of the three jets in the lab frame [28].

[27] J. Heinrich *et al.*, arXiv:physics/0409129v1.

[28] S. Geer and T. Asakawa, Phys. Rev., **D53**, 4793 (1996).